Computer Physics Communications 196 (2015) 36–44

Contents lists available at ScienceDirect

Computer Physics Communications

journal homepage: www.elsevier.com/locate/cpc

Optimization algorithm for the generation of ONCV pseudopotentials

Martin Schlipf*, François Gygi

Department of Computer Science, University of California Davis, Davis, CA 95616, USA

ARTICLE INFO

Article history:
Received 13 February 2015
Received in revised form
22 April 2015
Accepted 13 May 2015
Available online 29 May 2015

Keywords:
Density functional theory
Pseudopotential
Plane wave
All-electron calculation
Condensed matter

ABSTRACT

We present an optimization algorithm to construct pseudopotentials and use it to generate a set of Optimized Norm-Conserving Vanderbilt (ONCV) pseudopotentials for elements up to Z = 83 (Bi) (excluding Lanthanides). We introduce a quality function that assesses the agreement of a pseudopotential calculation with all-electron FLAPW results, and the necessary plane-wave energy cutoff. This quality function allows us to use a Nelder–Mead optimization algorithm on a training set of materials to optimize the input parameters of the pseudopotential construction for most of the periodic table. We control the accuracy of the resulting pseudopotentials on a test set of materials independent of the training set. We find that the automatically constructed pseudopotentials (http://www.quantum-simulation.org) provide a good agreement with the all-electron results obtained using the FLEUR code with a plane-wave energy cutoff of approximately 60 Ry.

1. Introduction

Pseudopotentials were introduced over three decades ago as an elegant simplification of electronic structure computations [1]. They allow one to avoid the calculation of electronic states associated with core electrons, and focus instead on valence electrons that most often dominate phenomena of interest, in particular chemical bonding. In the context of Density Functional Theory (DFT), pseudopotentials have made it possible to solve the Kohn–Sham equations [2,3] using a plane-wave basis set, which considerably reduces the complexity of calculations, and allows for the use of efficient Fast Fourier Transform (FFT) algorithms. The introduction of norm-conserving pseudopotentials (NCPPs) by Hamann et al. in 1979 [4,5] greatly improved the accuracy of DFT plane wave calculations by imposing a constraint (norm conservation) in the construction of the potentials, thus improving the transferability of potentials to different chemical environments. More elaborate representations of pseudopotentials were later proposed, most notably ultrasoft pseudopotentials [6] (USPPs) and the projector augmented wave [7] (PAW) method, improving computational efficiency by reducing the required plane wave energy cutoff. The implementation of these PPs is however more complex than NCPPs [8]. In particular for advanced calculations involving hybrid density functionals [9], many-body perturbation theory [10], or density-functional perturbation theory [11] terms treating the additional on-site contributions have to be developed [12]. Both USPPs and PAWs have been used with great success in a large number of computational studies published over the past two decades. NCPPs were also widely used but suffered from the need to use a large plane wave basis set for some elements, especially transition metals.

Recently, Hamann suggested [8] a method to construct optimized norm-conserving Vanderbilt (ONCV) potentials following the USPP construction algorithm without forfeiting the norm-conservation. The resulting potentials have an accuracy comparable to the USPPs at a moderately increased plane-wave energy cutoff.

Since the very first pseudopotentials were introduced, there has been an interest in a database of transferable, reference potentials that could be applied for many elements in the periodic table [5,13,14]. The need for a systematic database in high-throughput calculations led to a recent revival of this field: Garrity et al. [15] proposed a new set of USPPs for the whole periodic table except the noble gases and the rare earths. Dal Corso [16] constructed a high- and a low-accuracy PAW set for all elements up to Pu. Common to these approaches is the fact that the input parameters of the PP construction are selected by experience based on the results of the all-electron (AE) calculation of the bare atom. The quality of the constructed PP is then tested by an evaluation of different crystal structures and by comparing to the all-electron FLAPW [17–19] results. To standardize the testing procedure, Lejaeghere et al. [20] suggested to compare the area between a Murnaghan fit [21] obtained with the PP and the AE calculation resulting in a quality factor Δ. Küçükbenli et al. [22] proposed a crystalline monoatomic solid test, where this quality factor is evaluated for the simple cubic (sc), body-centered cubic (bcc), and face-centered cubic (fcc)

* Corresponding author.
E-mail addresses: martin.schlipf@gmail.com (M. Schlipf), fgygi@ucdavis.edu (F. Gygi).

http://dx.doi.org/10.1016/j.cpc.2015.05.011

structure to assess the quality of a PP. There are two improvements over these construction principles that we propose to address in this work. First, we introduce a quality function that takes into account the computational efficiency of the PP as well as its accuracy. Second, we allow for a systematic feedback of this quality function onto the input parameters defining the PP. In this way, we can introduce an automatic construction algorithm that optimizes the properties of the PP without bias from the constructor. We apply this algorithm to construct ONCV pseudopotentials and compare their performance with recent USPP [15] and PAW [16] PP libraries. The pseudopotentials are available in UPF and XML format on our webpage [23].

This paper is organized as follows: In Section 2, we outline the properties of the ONCV PPs and introduce the input parameters that will be optimized by the algorithm. In Section 3, we introduce the quality function to assess the performance of a PP, specify the materials we use to construct and test a PP, outline the setting of the DFT calculation, and finally present the optimization algorithm that iterates construction and testing until a good PP is found. We compare the constructed PPs to results obtained with the FLAPW, the USPP, and the PAW method in Section 4 and draw our conclusions in Section 5.

2. ONCV pseudopotentials

The optimized norm-conserving Vanderbilt (ONCV) pseudopotentials were recently proposed by Hamann [8]. Here, we briefly sketch their construction, following Hamann, to highlight the input parameters (bold in text) that determine the properties of the PP. The general idea is to introduce an **upper limit** wave vector q_c and optimize the pseudo wave functions $\varphi_i(r)$ such that the residual kinetic energy

$$E_{ij}(q_c) = \int_{q_c}^{\infty} \mathrm{d}q q^4 \varphi_i(q)\varphi_j(q) \tag{1}$$

above this cutoff is minimized. Here, $\varphi_i(q)$ is the Fourier transform of the pseudo wave function

$$\varphi_i(q) = 4\pi \int_0^{\infty} \mathrm{d}r r^2\, \mathrm{j}_l(qr)\varphi_i(r), \tag{2}$$

$\mathrm{j}_l(qr)$ a spherical Bessel function, and l the angular momentum of the pseudo wave function. On the one hand, the cutoff q_c determines which features of the physical potential can be described by the PP. On the other hand, increasing q_c makes the PP harder and hence more costly to evaluate.

For every angular momentum, a **projector radius** r_c determines in which region the pseudoization is done. The projector radius is approximately inversely proportional to the cutoff q_c so that a smaller value increases the computational cost along with the accuracy. Outside of this radius the wave function should follow the true all-electron wave function ψ. To ensure the continuity at this radius, one imposes M constraints on the continuity of the pseudo wave function

$$\left.\frac{\mathrm{d}^n\varphi}{\mathrm{d}r^n}\right|_{r_c} = \left.\frac{\mathrm{d}^n\psi}{\mathrm{d}r^n}\right|_{r_c}, \tag{3}$$

for $n = 0, \ldots, M-1$. In this work, we use $M = 5$ for all constructed PPs.

The basis set used in the optimization is constructed from spherical Bessel functions. As the basis functions are only used inside the sphere, they are set to zero outside of the projector radius. This destroys the orthogonality of the basis, so that one needs to orthogonalize it again. A linear combination of the orthogonalized basis functions yields a new basis where a single basis function φ_0 satisfies the constraints in Eq. (3) and for all other basis functions ξ_n^{N} the value and the $M-1$ derivatives at r_c are zero. As a consequence, the sum of φ_0 and any linear combination of the ξ_n^{N} will satisfy the constraints in Eq. (3). It is advantageous to select those linear combinations of ξ_n^{N} that have a maximal impact on the residual energy by evaluating the eigenvalues e_n and eigenvectors ξ_n^{R}

$$\varphi_i = \varphi_0 + \sum_{n=1}^{N-M} x_n \xi_n^{\mathrm{R}}. \tag{4}$$

In this work, we construct the PPs with $N = 8$ basis functions. Notice that the optimization of the pseudo wave function is performed under the constraint that the norm of the all-electron wave function is conserved

$$\int_0^{r_c} \mathrm{d}r r^2 \left[\varphi_i^*(r)\varphi_j(r) - \psi_i^*(r)\psi_j(r)\right] = 0. \tag{5}$$

From the obtained pseudo wave functions, one can construct projectors χ_i

$$\chi_i(r) = (\varepsilon_i - T - V_{\mathrm{loc}})\phi_i(r), \tag{6}$$

where T is the kinetic energy operator. V_{loc} is the local potential that follows the all-electron potential outside of r_c and is extended smoothly to the origin by a polynomial. For occupied states ε_i is the eigenvalue of the all-electron calculation. For unoccupied states, one needs to specify this **energy shift** before the construction of the PP. Following Ref. [8], we construct two projectors per angular momentum $l \le l_{\max}$ and only the local potential for all $l > l_{\max}$ above. The projectors define the following nonlocal potential

$$V_{\mathrm{NL}} = \sum_{ij} |\chi_i\rangle B_{ij}^{-1} \langle\chi_j| \tag{7}$$

where

$$B_{ij} = \langle\varphi_i|\chi_j\rangle, \tag{8}$$

which is a Hermitian matrix when normconserving pseudo wave functions are constructed [6]. One can simplify this potential by a unitary transformation to the eigenspace of the B matrix.

3. Computational details

3.1. Quality function

In order to employ numerical optimization algorithms in the construction of PPs, we need a function that maps the multidimensional input parameter space onto a single number, the *quality* of the PP. A good PP is characterized by a small relative deviation

$$\delta_{a_{\mathrm{lat}}}^{\mathrm{PP}} = a_{\mathrm{lat}}^{\mathrm{PP}}/a_{\mathrm{lat}}^{\mathrm{AE}} - 1 \tag{9}$$

between the lattice constant obtained in the plane-wave PP calculation $a_{\mathrm{lat}}^{\mathrm{PP}}$ and in the AE calculation $a_{\mathrm{lat}}^{\mathrm{AE}}$, respectively. A second criterion is the plane-wave energy cutoff E_{cut} necessary to converge the PP calculation. These two criteria compete with each other because the pseudoization of the potential reduces the necessary energy cutoff at the cost of a lower accuracy near the nucleus. Hence, we need to specify a target accuracy δ_0 which we want to achieve for our PPs, i.e., for all materials $\left|\delta_{a_{\mathrm{lat}}}^{\mathrm{PP}}\right| \le \delta_0$. We select $\delta_0 = 0.2\%$ motivated by the fact that the choice of different codes or input parameters in the all-electron calculation may already lead to a relative error of approximately 0.1%. To discriminate between PPs within the target accuracy, we include a term $\propto 1/E_{\mathrm{cut}}$ in the quality function, favoring smoother PPs over hard ones. For PPs that are significantly outside $\left|\delta_{a_{\mathrm{lat}}}^{\mathrm{PP}}\right| > 2\delta_0$ our target accuracy, we only focus on optimizing the relative deviation by an $1/(\delta_{a_{\mathrm{lat}}}^{\mathrm{PP}})^2$ term. We choose a smooth continuation between the two regions, resulting in the

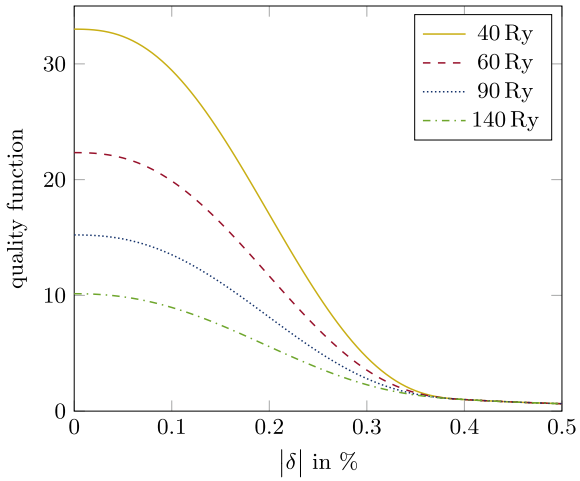

Fig. 1. (Color online) Quality function for various energy-cutoffs E_{cut}. For small δ, it is proportional to $1/E_{\text{cut}}$; for large δ proportional to $1/\delta^2$ and independent of E_{cut}.

function depicted in Fig. 1. The quality function has the following form

$$q(\delta, E_{\text{cut}}) = \begin{cases} A + C\delta^2 + D\delta^3 + E\delta^4 + F\delta^5 & \delta < 2\delta_0 \\ (2\delta_0/\delta)^2 & \delta \geq 2\delta_0 \end{cases} \tag{10}$$

with

$$A = 1 + \frac{1280}{E_{\text{cut}}} \qquad y_0 = 1 + \frac{680}{E_{\text{cut}}}$$

$$C = \frac{32y_0 - 16A - 29}{4\delta_0^3} \qquad D = \frac{19A - 48y_0 + 54}{4\delta_0^2}$$

$$E = \frac{96y_0 - 33A - 122}{16\delta_0^4} \qquad F = \frac{5A - 16y_0 + 22}{16\delta_0^5}.$$

The function can be multiplied by an arbitrary scaling constant, which we set such that the value of the quality function is 1 at $\left|\delta^{\text{PP}}_{a_{\text{lat}}}\right| = 2\delta_0$.

3.2. Sets of materials

As the constructed pseudopotentials depend on the set of materials used in the optimization algorithm, it is important that the set contain physically relevant environments of the atom. Furthermore, we select highly symmetric structures with at most two atoms per unit cell to reduce the computation time. As representatives of a metallic environment, we select the simple cubic (sc), the body-centered cubic (bcc), the face-centered cubic (fcc), and the diamond-cubic (dc) structure. Ionic environments are provided in a rock-salt or zinc-blende structure, where we combine elements such that they assume their most common oxidation state. This leads to a combination of elements from the lithium group with the fluorine group, the beryllium group with the oxygen group, and so on. We always use the three smallest elements of the respective groups to guarantee a variation in size of the resulting compounds. For the transition metals, several oxidation states are often possible. Hence, we combine them with carbon, nitrogen, and oxygen to test these different valencies. As the noble gases do not form compounds, we test them only in the sc, bcc, fcc, and dc structure.

Finally, we need to separate these materials into two sets. The *training set* consists of the bcc, and the fcc structure as well as all rock-salt compounds. It is used in the optimization algorithm to construct the PPs. As the PPs are specifically optimized to reproduce the structural properties of the training set, we can only judge if the PPs are highly accurate by calculating an independent *test set*. The test set contains the sc and the dc structure as well as all zinc-blende compounds. In total, the training and test sets consist of 602 materials, where every noble-gas atom is part of four materials, and every other element is part of at least ten materials.

3.3. Computational setup

All pseudopotentials are constructed using the Perdew–Burke–Ernzerhof (PBE) generalized gradient density functional [24]. We use an $8 \times 8 \times 8$ Monkhorst–Pack $\boldsymbol{k}$-point mesh in the AE as well as in the PP calculation. While this may not be sufficient to completely converge the lattice constant with respect to the numbers of $\boldsymbol{k}$-points, the errors in the PP and the AE calculation are expected to be the same, so that we can still compare the results. To ensure that metallic systems converge, we use a Fermi-type smearing with a temperature of 315.8 K corresponding to an energy of 0.001 htr.

For the AE calculation, we use the FLAPW method as implemented in the `Fleur` code [25]. We converge the plane-wave cutoff and add unoccupied local orbitals to provide sufficient variational freedom inside the muffin-tin spheres. The precise numerical values necessary to converge the calculation are different for every material; all input files can be obtained from our web page [23]. We obtain the lattice constant by a Murnaghan fit [21] through 11 data points surrounding the minimum of the total energy. We converge the AE lattice constant such that the relative error is at most 0.1%. There are methodological limitations of the FLAPW method that make a higher accuracy difficult to obtain for some elements: (i) On the one hand, only core states are treated fully relativistically. On the other hand, the non-spherical parts of the potential are only taken into account for valence states. (ii) Because the plane-waves only exist in the interstitial region, the maximum number of basis functions is limited to avoid linear dependence of the basis set. (iii) The additional basis functions in the muffin-tin spheres must be linearly independent, limiting the minimal energy parameter for these functions.

The automatic construction of pseudopotentials requires every material to be calculated several hundred times. Hence, we approximate the Murnaghan equation of state by a parabola that we fit through data points at the AE lattice constant and a 1% enlarged or reduced value. We test the constructed PPs with the QUANTUM ESPRESSO [26] plane-wave DFT code. Our test consists of a calculation with a large energy cutoff of $E^{\text{max}}_{\text{cut}} = 160$ Ry that we consider to be the converged solution. Then, we decrease the cutoff in steps of $\Delta E = 10$ Ry to the minimum of 40 Ry. Notice that as illustrated by Fig. 2, the actual deviation compared to the AE calculation may decrease even though we reduced the accuracy of the calculation. To correct for this, we adjust the deviation such that it is monotonically decreasing using the following correction

$$\delta^{\text{PP}}_{\text{corr}}(E^i_{\text{cut}}) = |\delta^{\text{PP}}(E^{\text{max}}_{\text{cut}})| + \sum_{k=1}^{i} |\delta^{\text{PP}}(E^k_{\text{cut}}) - \delta^{\text{PP}}(E^{k-1}_{\text{cut}})| \tag{11}$$

where $E^i_{\text{cut}} = E^{\text{max}}_{\text{cut}} - 10i$. This ensures that the deviation at a given cutoff energy is an upper bound to the deviation at any larger cutoff.

3.4. Optimizing pseudopotentials

We use a Nelder–Mead algorithm [27] also known as the Downhill Simplex Method [28] to optimize the PPs. In this algorithm, the N input parameters of a specific PP are represented by a point in a N-dimensional space. We start with $(N + 1)$ PPs that form a simplex in this space. By replacing the worst corner by a better PP the simplex contracts towards the optimal PP. As convergence criteria, we visually inspect the change of quality of the PP. In addition, we require that the input parameters of the PP are converged to

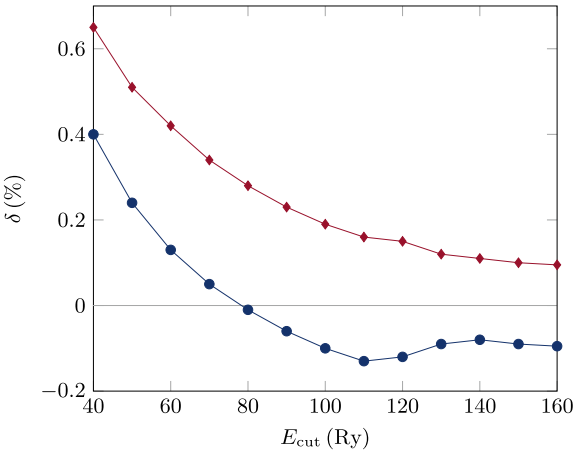

Fig. 2. (Color online) Relative deviation δ of a PP w.r.t. the AE calculation. The blue circles indicate the deviation obtained at a certain energy cutoff E_{cut}. The red diamonds show the corrected deviation that is monotonically decreasing with increasing cutoff (see text).

at least two significant digits. The advantages of the Nelder–Mead algorithm are that we do not need to know the derivatives of the quality function with respect to the input parameters and that it can find PP parameters that lie outside of the starting simplex.

To create the initial simplex, we start from a reasonable starting guess for the N input parameters to construct a PP for the neutral atom. We used the example input files provided with the ONCVPSP package [8], where available, or generated our own PP otherwise. States that could be considered as semicore states are included in the valence window. A detailed list for the individual elements is given in the supplementary material [29]. We construct $(N + 1)$ PPs based on the starting-guess PP with random modifications to the input parameters. We allow changes of up to 20% of any of the input parameters, but control that the necessary conditions (e.g. projector radius $\geq$ radius of local potential) are always fulfilled.

We assess the quality for each of the initial PPs and each of the PPs that are created during the optimization procedure in the following fashion: (i) The PP is rejected if it cannot be created by the ONCVPSP code or if it exhibits ghost states in the vicinity of the Fermi energy. The latter is evidenced by changes in the logarithmic derivative as compared to the AE result. (ii) If the PP is not rejected, we evaluate the quality function on the training set of materials. (iii) We compute the geometric mean of all the materials the tested PP is used in.

In the case of the rock-salt compounds, we test always only one of the PP and for the other element we use a PP from the GBRV database [15]. After 80–200 iterations of the Nelder–Mead algorithm, all PPs have converged. Then, we restart the algorithm using these first generation PP as starting guess. Now, we employ the first generation PPs in the compounds so that our resulting PPs become independent of the GBRV database. Once the second generation is converged as well (another 100 iterations), the properties of the training set are well reproduced for almost all materials.

3.5. Refining the training set

For a few materials, the second generation PPs do not reproduce the AE results on the test set of materials. Our proposed optimization algorithm provides an easy solution to overcome these cases by adding additional materials to the training set. In particular, for the early transition metals (Sc–Mn) it is necessary to include the sc structure in the training set. Furthermore, we include the dimer of hydrogen and nitrogen into the test set, because the second generation PPs for these two elements do not describe the bond length of the dimer accurately.

We emphasize that our optimization algorithm could account for other material properties. As long as one is able to define a quality function, which maps the result of a PP potential calculation onto a number, it is possible to optimize the input parameters of the PP generation by standard numerical optimization techniques.

Table 1
Comparison of the performance of the USPPs in the GBRV database [15] and the high-accuracy PAWs in PSLIB [16] with the ONCV PPs in the SG15 database (this work) for materials in a bcc structure. We analyze the relative deviation of the lattice constant $\delta_{a_{\text{lat}}}$ and the bulk modulus δ_{B_0} between a PP and the AE calculation. The average reveals if the PPs have a systematic bias and the root-mean-square (rms) average tests the size of the error. We also show the proportion of materials that are not accurately described at various energy cutoffs.

	GBRV	PSLIB	SG15
Average $\delta_{a_{\text{lat}}}$ (%)	0.03	0.03	0.04
rms average $\delta_{a_{\text{lat}}}$ (%)	0.12	0.11	0.08
% of materials with $\lvert\delta_{a_{\text{lat}}}\rvert > 0.2\%$[1]	10.94	40.00	23.19
% of materials with $\lvert\delta_{a_{\text{lat}}}\rvert > 0.2\%$[2]	9.38	15.56	8.70
% of materials with $\lvert\delta_{a_{\text{lat}}}\rvert > 0.2\%$[3]	9.38	4.44	2.90
Average δ_{B_0} (%)	0.36	−0.32	0.52
rms average δ_{B_0} (%)	3.31	2.53	3.19
% of materials with $\lvert\delta_{B_0}\rvert > 5.0\%$[1]	25.00	62.22	53.62
% of materials with $\lvert\delta_{B_0}\rvert > 5.0\%$[2]	14.06	26.67	18.84
% of materials with $\lvert\delta_{B_0}\rvert > 5.0\%$[3]	9.38	8.89	7.25
Total number of materials	64	45	69

[1] With an energy cutoff of 40Ry.
[2] With an energy cutoff of 60Ry.
[3] With an energy cutoff of 160Ry.

4. Results

We compare the performance of the ONCV PPs constructed in this work (SG15) [23] with the USPPs in the GBRV database [15] and the high-accuracy PAWs in the PSLIB [16]. For the latter, we generate the potentials of PSLIB version 1.0.0 with QUANTUM ESPRESSO version 5.1.1. When we state that a certain pseudoization has a particular convergence behavior, we refer to the properties of the PPs in these libraries.

In the first subsection, we focus on the lattice constants and bulk moduli of the materials in the training set. In the second subsection, we investigate the materials in the test set. In the third subsection, we look into materials that are not represented in the test set to check the accuracy of the pseudopotentials. In the first two subsections, we focus only on the trends across all materials in the training and test set, respectively. For the results for a specific compound, please refer to the supplementary material [29].

4.1. Training set

In Table 1, we present the results obtained for the materials in a bcc structure. We see that the USPPs require the smallest energy cutoff and have the best performance at 40 Ry. On the other hand increasing the energy cutoff beyond 40 Ry hardly improves the results. For the PAWs and the ONCV PPs, a large number of materials are not converged at 40 Ry, but increasing the energy cutoff improves the accuracy, so that they are able to improve on the USPP results. For the converged calculation, the root-mean-square (rms) error is around 0.1% for all PPs and smallest for the ONCV PPs. We see a similar trend for the bulk moduli though the converged results require a larger energy cutoff on average. The average error for the converged bulk moduli is roughly 3% and the USPPs converge with a lower energy cutoff than the PAWs and the ONCV PPs, which have a similar convergence behavior. In Fig. 3, we see that the converged lattice constant deviates by more than 0.2% with the ONCV PPs only for two materials (carbon and calcium).

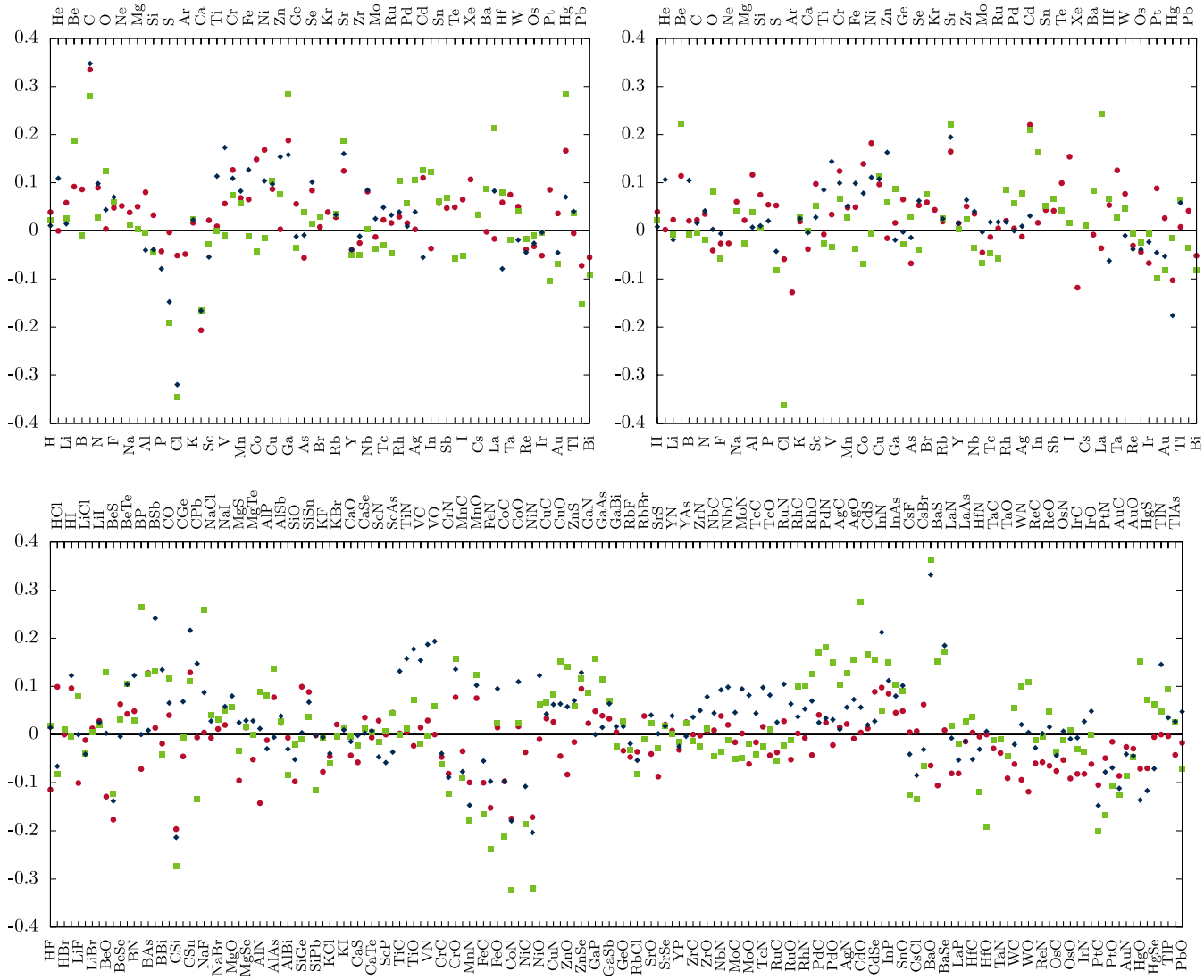

Fig. 3. (Color online) Relative change $\delta(\%)$ of the lattice constant in the training set for the SG15 (red circle), the GBRV (green square), and the PSLIB (blue diamond) results as compared to the FLAPW ones for the bcc (top left), fcc (top right) and rock-salt compounds (bottom).

Table 2
Same as Table 1 for fcc structures.

	GBRV	PSLIB	SG15
Average $\delta_{a_{\text{lat}}}$ (%)	0.03	0.03	0.03
rms average $\delta_{a_{\text{lat}}}$ (%)	0.11	0.07	0.07
% of materials with $\lvert\delta_{a_{\text{lat}}}\rvert > 0.2\%$[1]	9.38	27.08	24.64
% of materials with $\lvert\delta_{a_{\text{lat}}}\rvert > 0.2\%$[2]	9.38	6.25	5.80
% of materials with $\lvert\delta_{a_{\text{lat}}}\rvert > 0.2\%$[3]	9.38	0.00	1.45
Average δ_{B_0} (%)	0.23	0.00	0.31
rms average δ_{B_0} (%)	2.28	1.83	2.00
% of materials with $\lvert\delta_{B_0}\rvert > 5.0\%$[1]	12.50	68.75	43.48
% of materials with $\lvert\delta_{B_0}\rvert > 5.0\%$[2]	7.81	16.67	17.39
% of materials with $\lvert\delta_{B_0}\rvert > 5.0\%$[3]	3.12	4.17	5.80
Total number of materials	64	48	69

[1] With an energy cutoff of 40Ry.
[2] With an energy cutoff of 60Ry.
[3] With an energy cutoff of 160Ry.

For both of these materials the USPP and the PAW approach show large deviations as well.

The fcc structures presented in Table 2 follow the same trend as the bcc structures. The USPPs require the smallest energy cutoff but cannot be improved further by increasing the energy cutoff. The PAWs and the ONCV PPs require an energy cutoff of 60 Ry to converge most materials, but have fewer inaccurate elements when increasing the energy cutoff. Overall the ONCV PPs and the PAWs are a bit better than the USPPs, but all PPs are close to the AE results. In Fig. 3, we see that only a single material (cadmium) is outside the 0.2% boundary, when using the converged calculation and the ONCV PPs. The USPP result shows a deviation of similar size for this material, whereas the PAW lattice constant is close to the FLAPW result.

When combining two materials to form rock-salt compounds, we obtain the results depicted in Table 3. In comparison to the metallic (bcc and fcc) system, the accuracy for the ionic compounds is a bit higher in particular for the bulk modulus. With a large energy cutoff the ONCV PPs essentially reproduce the AE results and the accuracy at 60 Ry for the lattice constant is very good. For the bulk modulus, about 10% of the materials require a larger energy cutoff. The USPPs have a slightly larger mismatch for the lattice constants, but converge both lattice constants and bulk moduli with 40 Ry. The PAW potentials provide a similar convergence behavior as the ONCV potentials; they deviate a bit more for the lattice constants, but provide slightly better bulk moduli.

In Fig. 4, we show a histogram of the relative error of the lattice constant for all the examined PPs (with the converged cutoff of

Table 3
Same as Table 1 for rocksalt structures.

	GBRV	PSLIB	SG15
Average $\delta_{a_{\mathrm{lat}}}$ (%)	0.01	0.02	−0.02
rms average $\delta_{a_{\mathrm{lat}}}$ (%)	0.11	0.09	0.06
% of materials with $\lvert\delta_{a_{\mathrm{lat}}}\rvert > 0.2\%$[1]	6.13	35.95	30.67
% of materials with $\lvert\delta_{a_{\mathrm{lat}}}\rvert > 0.2\%$[2]	6.13	6.54	1.23
% of materials with $\lvert\delta_{a_{\mathrm{lat}}}\rvert > 0.2\%$[3]	6.13	3.92	0.00
Average δ_{B_0} (%)	−0.02	−0.03	−0.48
rms average δ_{B_0} (%)	1.67	1.29	1.34
% of materials with $\lvert\delta_{B_0}\rvert > 5.0\%$[1]	1.84	53.59	55.83
% of materials with $\lvert\delta_{B_0}\rvert > 5.0\%$[2]	1.84	5.23	10.43
% of materials with $\lvert\delta_{B_0}\rvert > 5.0\%$[3]	1.84	0.00	0.61
Total number of materials	163	153	163

[1] With an energy cutoff of 40Ry.
[2] With an energy cutoff of 60Ry.
[3] With an energy cutoff of 160Ry.

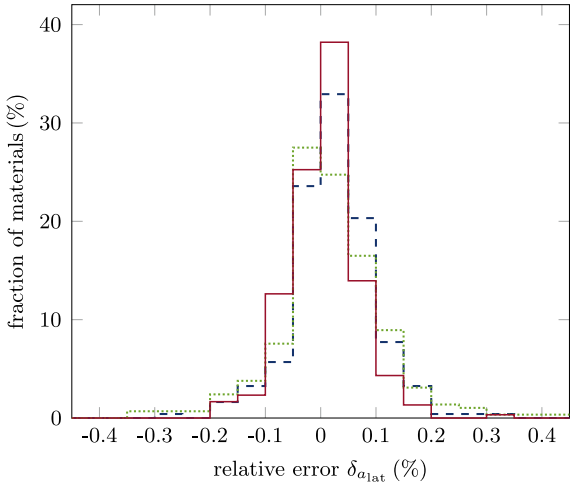

Fig. 4. (Color online) Histogram of the relative error of the lattice constant compared to the all-electron result. We show the results for all materials in the training set for the SG15 (red solid line), the GBRV (green dotted line), and the PSLIB (blue dashed line) calculations.

160 Ry). The histogram confirms the conclusions we drew from Table 1 to 3: All PPs show a very good agreement with the all-electron results and the USPPs have a slightly lower accuracy. The tails with large errors are very flat indicating that there are only a few outliers.

4.2. Test set

In the sc structure (see Table 4), the performance of the ONCV potentials is comparable to the training set for the lattice constants and slightly worse for the bulk moduli. We observe the same trend also for the USPP and the PAW calculations. With an overall deviation of about 0.1% for the lattice constant and 4% for the bulk moduli, all PPs show a good agreement with the AE reference data. The convergence with respect to the energy cutoff is best in the GBRV database, which does not change significantly for the lattice constants above 40 Ry. Most of the ONCV lattice constants converge at 60 Ry whereas the PAW ones occasionally need a larger cutoff. For the bulk moduli, all PPs show a similar convergence behavior. However, we observe that as compared to the other structures a larger fraction of $>$ 10% is not accurate even with an energy cutoff of 160 Ry. In Fig. 5, we see that the ONCV PPs reproduce the lattice constant within the 0.2% boundary for all materials except calcium and lanthanum. While the ONCV PP gives similar results to the other PPs for calcium, we find that the lattice constant in lanthanum is underestimated by the ONCV PP and

Table 4
Same as Table 1 for sc structures.

	GBRV	PSLIB	SG15
Average $\delta_{a_{\mathrm{lat}}}$ (%)	0.02	0.03	0.02
rms average $\delta_{a_{\mathrm{lat}}}$ (%)	0.12	0.09	0.09
% of materials with $\lvert\delta_{a_{\mathrm{lat}}}\rvert > 0.2\%$[1]	6.25	46.30	27.54
% of materials with $\lvert\delta_{a_{\mathrm{lat}}}\rvert > 0.2\%$[2]	6.25	16.67	5.80
% of materials with $\lvert\delta_{a_{\mathrm{lat}}}\rvert > 0.2\%$[3]	6.25	3.70	2.90
Average δ_{B_0} (%)	0.32	0.31	−0.01
rms average δ_{B_0} (%)	3.79	3.96	4.47
% of materials with $\lvert\delta_{B_0}\rvert > 5.0\%$[1]	40.62	74.07	62.32
% of materials with $\lvert\delta_{B_0}\rvert > 5.0\%$[2]	20.31	27.78	21.74
% of materials with $\lvert\delta_{B_0}\rvert > 5.0\%$[3]	12.50	12.96	11.59
Total number of materials	64	54	69

[1] With an energy cutoff of 40Ry.
[2] With an energy cutoff of 60Ry.
[3] With an energy cutoff of 160Ry.

Table 5
Same as Table 1 for diamond structures.

	GBRV	PSLIB	SG15
Average $\delta_{a_{\mathrm{lat}}}$ (%)	0.03	0.02	0.01
rms average $\delta_{a_{\mathrm{lat}}}$ (%)	0.16	0.10	0.12
% of materials with $\lvert\delta_{a_{\mathrm{lat}}}\rvert > 0.2\%$[1]	7.81	49.12	34.78
% of materials with $\lvert\delta_{a_{\mathrm{lat}}}\rvert > 0.2\%$[2]	7.81	22.81	11.59
% of materials with $\lvert\delta_{a_{\mathrm{lat}}}\rvert > 0.2\%$[3]	7.81	7.02	8.70
Average δ_{B_0} (%)	0.45	1.30	−0.24
rms average δ_{B_0} (%)	4.49	6.54	3.06
% of materials with $\lvert\delta_{B_0}\rvert > 5.0\%$[1]	31.25	71.93	53.62
% of materials with $\lvert\delta_{B_0}\rvert > 5.0\%$[2]	18.75	31.58	14.49
% of materials with $\lvert\delta_{B_0}\rvert > 5.0\%$[3]	9.38	7.02	7.25
Total number of materials	64	57	69

[1] With an energy cutoff of 40Ry.
[2] With an energy cutoff of 60Ry.
[3] With an energy cutoff of 160Ry.

overestimated by the USPP. For this material, the PAW calculation did not converge.

In Table 5, we present our results for the materials in the diamond structure. These are the structures which exhibit overall the largest deviation from the all-electron result. The lattice constants of the USPPs are converged well with the energy cutoff of 40 Ry, whereas the PAWs and the ONCV PPs frequently require a cutoff of 60 Ry. For the bulk moduli, we find that the ONCV PPs provide the best agreement with the AE results. The quality of the USPPs is similar, but the PAW potentials show an average error larger than the desired 5% tolerance. However the fraction of materials that are well described with the PP calculation is similar for all methods. This indicates that a few specific materials show a particular large deviation, whereas the rest is accurately described. For the ONCV PPs the lattice constants of boron, chlorine, scandium, nickel, rubidium, and yttrium deviate by more than 0.2% from the FLAPW results. In Fig. 5, we observe that the deviations between the different pseudoizations are larger than for the other structures. A possible explanation is that the diamond structure is an extreme case for many materials, because of its low space filling.

For the zincblende compounds (cf. Table 6), we observe results similar to for the rock-salt compounds. We find that the USPPs converge for most materials with an energy cutoff of 40 Ry, whereas a third of the materials with the ONCV PPs and half of the materials with the PAWs need an energy cutoff of 60 Ry to converge. Overall the accuracy of the ONCV PPs is slightly better than the alternatives, but all pseudoizations are on average well below the target of 0.2%. For the bulk moduli a larger energy cutoff is necessary, but when converged the deviation from the AE results is around 1%. In Fig. 5, we identify that only for BeO the deviation between the ONCV calculation and the AE result is larger than 0.2%.

In Fig. 6, the histogram of the relative error of the lattice constant for the test set confirms the conclusions we drew from Table 4

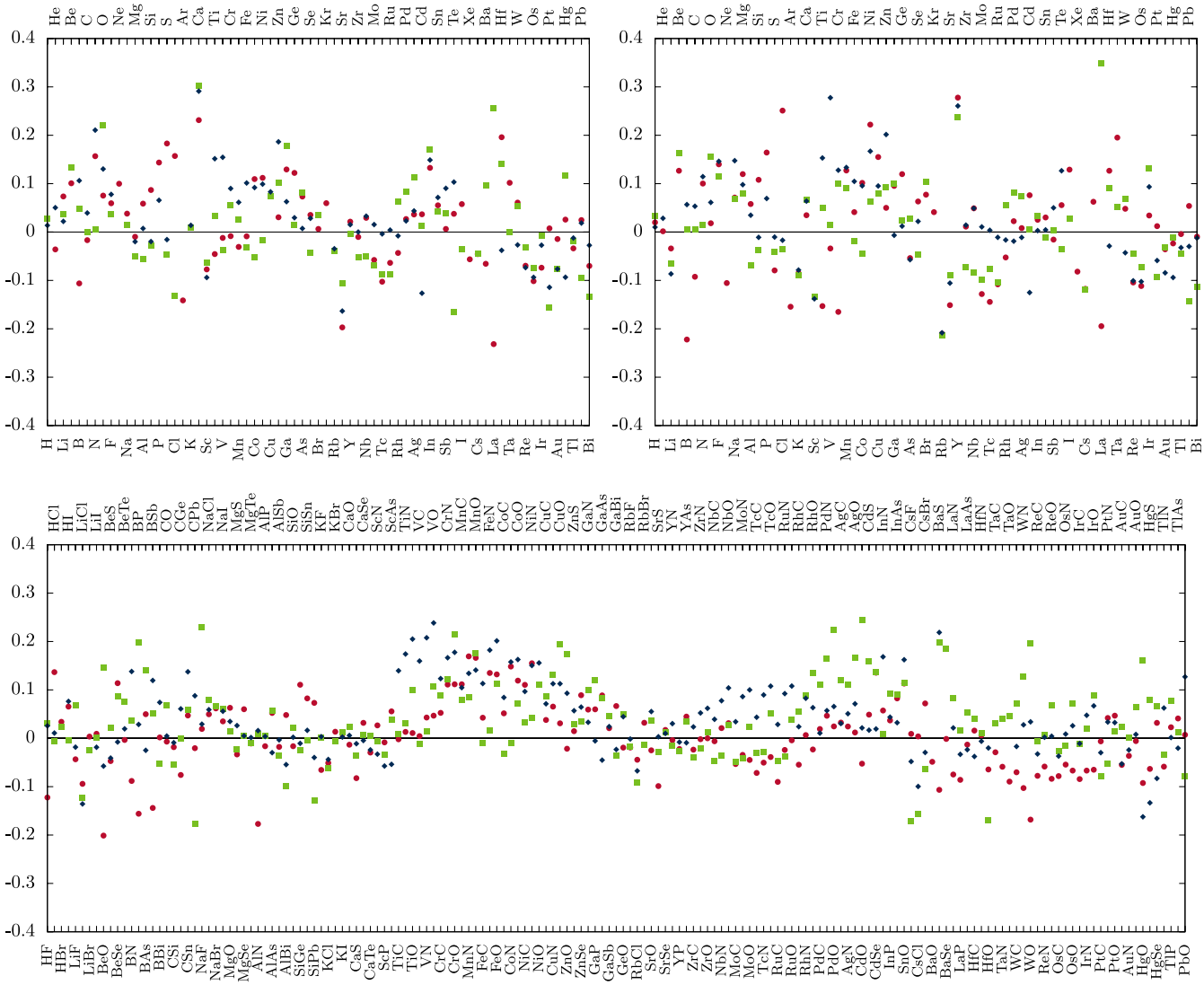

Fig. 5. (Color online) Relative change $\delta(\%)$ of the lattice constant in the test set for the SG15 (red circle), the GBRV (green square), and the PSLIB (blue diamond) results as compared to the FLAPW ones for the sc (top left), diamond (top right) and zincblende compounds (bottom).

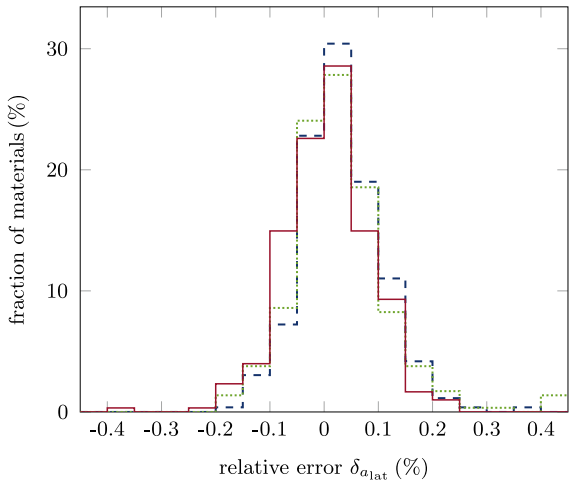

Fig. 6. (Color online) Histogram of the relative error of the lattice constant compared to the all-electron result. We show the results for all materials in the test set for the SG15 (red solid line), the GBRV (green dotted line), and the PSLIB (blue dashed line) calculations.

Table 6
Same as Table 1 for zincblende structures.

	GBRV	PSLIB	SG15
Average $\delta_{a_{\mathrm{lat}}}$ (%)	0.04	0.04	0.00
rms average $\delta_{a_{\mathrm{lat}}}$ (%)	0.10	0.09	0.07
% of materials with $\lvert\delta_{a_{\mathrm{lat}}}\rvert > 0.2\%$[1]	5.52	37.50	33.74
% of materials with $\lvert\delta_{a_{\mathrm{lat}}}\rvert > 0.2\%$[2]	4.91	6.58	2.45
% of materials with $\lvert\delta_{a_{\mathrm{lat}}}\rvert > 0.2\%$[3]	3.07	3.29	0.61
Average δ_{B_0} (%)	0.24	0.14	−0.27
rms average δ_{B_0} (%)	1.26	0.96	1.03
% of materials with $\lvert\delta_{B_0}\rvert > 5.0\%$[1]	4.29	55.26	55.21
% of materials with $\lvert\delta_{B_0}\rvert > 5.0\%$[2]	1.84	4.61	9.20
% of materials with $\lvert\delta_{B_0}\rvert > 5.0\%$[3]	0.61	0.00	0.00
Total number of materials	163	152	163

[1] With an energy cutoff of 40Ry.
[2] With an energy cutoff of 60Ry.
[3] With an energy cutoff of 160Ry.

to 6: The deviation from the all electron results is very small for all PPs. The USPPs show a slightly larger deviation than the PAWs and the ONCV PPs. The histogram reveals that this is partly due to some outliers, for which the lattice constant is overestimated by more than 0.4%. Overall, we notice that the accuracy of the ONCV PPs for

the test set of materials is not significantly worse than for the training set. Hence, we are confident that these PPs are transferable to other materials as well.

4.3. Dimers and ternary compounds

Our training and test set are limited to mono- and diatomic crystals, hence one may wonder if the constructed ONCV PPs work outside this scope. To test this we investigated diatomic molecules and ternary compounds. For the compounds, we use the same computational setup as for the materials in the training and in the test set. For the molecules, we optimize the bond length inside a box with dimensions 15 Å × 15 Å × 30 Å with the long side parallel to the axis of the molecule.

In Table 7, we show the bond lengths and the lattice constants of the investigated materials. Depending on the pseudoization, some diatomic molecules show large deviations from the reference data from the CCCB DataBase [30]. Overall, the ONCV PPs exhibit the smallest deviations. The relative error is larger than 0.2% only for the O_2 (0.25%) and the F_2 (0.35%) dimer. For the USPPs, all diatomic molecules are outside of the desired relative accuracy of 0.2%, except for the Br_2 dimer. In PAW, the only molecule with the desired accuracy is the H_2 dimer. The other molecules show deviations of similar magnitude to the USPPs and the Br_2 dimer did not converge.

Perovskites are accurately described by all pseudoizations; we frequently find a relative agreement of better than 0.1% in the lattice constant with the FLAPW result. The worst case for the ONCV PPs is $LaAlO_3$, which deviates by −0.13%. The USPPs and the PAWs both overestimate the lattice constant of $BaTiO_3$ by 0.25% and 0.27%, respectively. The PAW potentials also feature a larger deviation than the other two pseudoizations for $SrTiO_3$.

Finally, we consider the half-Heusler compounds. All materials are within the desired accuracy with all pseudoizations. The ONCV PPs show slightly larger deviations than the USPPs and the PAWs for GeAlCu and NMgLi. For NiScSb, the ONCV PPs and PAWs overestimate the lattice constant more than the USPPs. The lattice constant of BScSb and PdZrSn are essentially the same with FLAPW and in any pseudoization used. In PZNa, all PPs produce very similar results and a slightly larger lattice constant than the FLAPW result.

Table 7
Bond length of diatomic molecules and lattice constant of perovskites and half-Heusler compounds investigated with different methods. For the half-Heusler compounds, the first element is in Wyckoff position *c*. All values are given in Å.

Material	ref.[1]	GBRV	PSLIB	SG15
H_2	0.750	0.757	0.750	0.749
N_2	1.102	1.108	1.110	1.101
O_2	1.218	1.224	1.230	1.221
F_2	1.412	1.424	1.419	1.417
Cl_2	2.012	2.004	2.006	2.015
Br_2	2.311	2.311		2.314
$AsNCa_3$	4.764	4.765	4.764	4.764
$BaTiO_3$	4.018	4.028	4.029	4.020
$KMgCl_3$	5.024	5.023	5.025	5.023
$LaAlO_3$	3.814	3.817	3.815	3.809
$PNCa_3$	4.720	4.720	4.720	4.719
$SrTiO_3$	3.937	3.939	3.942	3.938
BScBe	5.318	5.319	5.316	5.317
GeAlCu	5.910	5.914	5.913	5.920
NiScSb	6.118	6.120	6.123	6.123
NMgLi	5.004	5.006	5.006	5.010
PdZrSn	6.392	6.392	6.394	6.394
PZnNa	6.141	6.149	6.148	6.148

[1] We evaluate the lattice constant perovskites and half Heusler with FLAPW and take the bond length of the dimers from the CCCB DataBase [30].

Table 8
Summary of the results depicted in Table 1 to 6 with same notation as Table 1.

	GBRV	PSLIB	SG15
Average $\delta_{a_{\mathrm{lat}}}$ (%)	0.03	0.03	0.01
rms average $\delta_{a_{\mathrm{lat}}}$ (%)	0.12	0.09	0.08
% of materials with $\lvert\delta_{a_{\mathrm{lat}}}\rvert > 0.2\%$[1]	7.04	38.51	30.07
% of materials with $\lvert\delta_{a_{\mathrm{lat}}}\rvert > 0.2\%$[2]	6.70	10.22	4.65
% of materials with $\lvert\delta_{a_{\mathrm{lat}}}\rvert > 0.2\%$[3]	6.19	3.73	1.99
Average δ_{B_0} (%)	0.21	0.18	−0.14
rms average δ_{B_0} (%)	2.61	2.85	2.40
% of materials with $\lvert\delta_{B_0}\rvert > 5.0\%$[1]	13.75	60.51	54.49
% of materials with $\lvert\delta_{B_0}\rvert > 5.0\%$[2]	7.73	13.36	13.62
% of materials with $\lvert\delta_{B_0}\rvert > 5.0\%$[3]	4.47	3.34	3.82
Total number of materials	582	509	602

[1] With an energy cutoff of 40Ry.
[2] With an energy cutoff of 60Ry.
[3] With an energy cutoff of 160Ry.

5. Conclusion

We have presented an algorithm to optimize the input parameters of a pseudopotential (PP) construction. We demonstrated it by developing the SG15 dataset [23] of ONCV pseudopotentials, which exhibits a similar accuracy as the ultrasoft PP database GBRV [15] and the PAW library PSLIB [16]. The idea of the algorithm is to map a PP onto a single numeric value so that standard optimization techniques can be employed. For this, we developed a quality function that considers the accuracy of the lattice constant of a PP calculation and compares it with a high accuracy FLAPW one. In addition, the quality function takes into account the energy cutoff necessary to converge the calculation. Hence, the optimization of the PPs with respect to the quality function yields accurate and efficient potentials. In order to ensure that the constructed PPs are of a high accuracy, we systematically chose a set of approximately 600 materials and evaluate their properties with FLAPW. We split this set in two parts, a training set used for the optimization of the PPs and a test set to analyze the performance of the PPs. When a PP does not produce our desired accuracy after optimizing on the training set, we can improve the quality of this PP by extending the training set by more materials.

In Table 8, we collect the results of all materials in test and training set. Compared to the PPs from the GBRV database [15] and PSLIB [16], the PPs in the SG15 set have the lowest root-mean-square deviation from the FLAPW results for the lattice constant. With an energy cutoff of 60 Ry, the ONCV PPs feature the least number of materials with an inaccurate lattice constant (deviation larger than 0.2% from FLAPW results). The advantage of the ultrasoft PPs is that they offer a similar accuracy with an energy cutoff of 40 Ry. For the bulk moduli larger energy cutoffs are necessary for all pseudoization methods. The ONCV PPs have the smallest root-mean-square deviation for the tested materials. The fraction of materials that can be accurately described with the ONCV PPs at a certain energy cutoff is very similar to the performance of the PAWs. The ultrasoft PPs exhibit a similar accuracy at a moderately lower energy cutoff. For materials that go beyond the training and test set, we find that the ONCV PPs provides the best description of diatomic molecules. All pseudopotentials are very accurate for perovskite and half-Heusler compounds.

We encourage the community to use the algorithm presented in this work to optimize pseudopotentials for different functionals and with different construction methods. With only a modest increase in the energy cutoff, the proposed SG15 library of norm-conserving pseudopotentials provides a competitive alternative to the libraries using USPP and PAW. As these pseudopotentials are less complex than the alternatives, this results in a great simplification in the development and implementation of new algorithms.

Acknowledgments

We would like to thank I. Castelli and N. Marzari for pointing out to us the importance of rejecting pseudopotentials with ghost states.

This work was supported by the US Department of Energy through grant DOE-BES DE-SC0008938. An award of computer time was provided by the DOE Innovative and Novel Computational Impact on Theory and Experiment (INCITE) program. This research used resources of the Argonne Leadership Computing Facility at Argonne National Laboratory, which is supported by the Office of Science of the US Department of Energy under contract DE-AC02-06CH11357.

Appendix A. Supplementary material

Supplementary material related to this article can be found online at http://dx.doi.org/10.1016/j.cpc.2015.05.011.

References

[1] R.M. Martin, Electronic Structure: Basic Theory and Practical Methods, Cambridge University Press, 2004.
[2] P. Hohenberg, W. Kohn, Phys. Rev. 136 (1964) B864. http://dx.doi.org/10.1103/PhysRev.136.B864.
[3] W. Kohn, L.J. Sham, Phys. Rev. 140 (1965) A1133. http://dx.doi.org/10.1103/PhysRev.140.A1133.
[4] D.R. Hamann, M. Schlüter, C. Chiang, Phys. Rev. Lett. 43 (1979) 1494. http://dx.doi.org/10.1103/PhysRevLett.43.1494.
[5] G.B. Bachelet, D.R. Hamann, M. Schlüter, Phys. Rev. B 26 (1982) 4199. http://dx.doi.org/10.1103/PhysRevB.26.4199.
[6] D. Vanderbilt, Phys. Rev. B 41 (1990) 7892. http://dx.doi.org/10.1103/PhysRevB.41.7892.
[7] P.E. Blöchl, Phys. Rev. B 50 (1994) 17953. http://dx.doi.org/10.1103/PhysRevB.50.17953.
[8] D.R. Hamann, Phys. Rev. B 88 (2013) 085117. http://dx.doi.org/10.1103/PhysRevB.88.085117.
[9] A.D. Becke, J. Chem. Phys. 98 (1993) 1372. http://dx.doi.org/10.1063/1.464304; A.D. Becke, J. Chem. Phys. 98 (1993) 5648.
[10] F. Aryasetiawan, O. Gunnarsson, Rep. Progr. Phys. 61 (1998) 237.
[11] S. Baroni, P. Giannozzi, A. Testa, Phys. Rev. Lett. 58 (1987) 1861. http://dx.doi.org/10.1103/PhysRevLett.58.1861.
[12] C. Audouze, F. m. c. Jollet, M. Torrent, X. Gonze, Phys. Rev. B 73 (2006) 235101. http://dx.doi.org/10.1103/PhysRevB.73.235101.
[13] N. Troullier, J.L. Martins, Phys. Rev. B 43 (1991) 1993. http://dx.doi.org/10.1103/PhysRevB.43.1993.
[14] C. Hartwigsen, S. Goedecker, J. Hutter, Phys. Rev. B 58 (1998) 3641. http://dx.doi.org/10.1103/PhysRevB.58.3641.
[15] K.F. Garrity, J.W. Bennett, K.M. Rabe, D. Vanderbilt, Comput. Mater. Sci. 81 (2014) 446. http://dx.doi.org/10.1016/j.commatsci.2013.08.053.
[16] A. Dal Corso, Comput. Mater. Sci. 95 (2014) 337. http://dx.doi.org/10.1016/j.commatsci.2014.07.043.
[17] E. Wimmer, H. Krakauer, M. Weinert, A.J. Freeman, Phys. Rev. B 24 (1981) 864. http://dx.doi.org/10.1103/PhysRevB.24.864.
[18] M. Weinert, E. Wimmer, A.J. Freeman, Phys. Rev. B 26 (1982) 4571. http://dx.doi.org/10.1103/PhysRevB.26.4571.
[19] H.J.F. Jansen, A.J. Freeman, Phys. Rev. B 30 (1984) 561. http://dx.doi.org/10.1103/PhysRevB.30.561.
[20] K. Lejaeghere, V. Van Speybroeck, G. Van Oost, S. Cottenier, Crit. Rev. Solid State Mater. Sci. 39 (2014) 1. http://dx.doi.org/10.1080/10408436.2013.772503.
[21] F. Murnaghan, Proc. Nat. Acad. Sci. USA 30 (1944) 244.
[22] E. Kucukbenli, M. Monni, B. Adetunji, X. Ge, G. Adebayo, N. Marzari, S. de Gironcoli, A.D. Corso, arXiv:1404.3015.
[23] http://www.quantum-simulation.org.
[24] J.P. Perdew, K. Burke, M. Ernzerhof, Phys. Rev. Lett. 77 (1996) 3865. http://dx.doi.org/10.1103/PhysRevLett.77.3865.
[25] http://www.flapw.de.
[26] P. Giannozzi, S. Baroni, N. Bonini, M. Calandra, R. Car, C. Cavazzoni, D. Ceresoli, G.L. Chiarotti, M. Cococcioni, I. Dabo, A. Dal Corso, S. de Gironcoli, S. Fabris, G. Fratesi, R. Gebauer, U. Gerstmann, C. Gougoussis, A. Kokalj, M. Lazzeri, L. Martin-Samos, N. Marzari, F. Mauri, R. Mazzarello, S. Paolini, A. Pasquarello, L. Paulatto, C. Sbraccia, S. Scandolo, G. Sclauzero, A.P. Seitsonen, A. Smogunov, P. Umari, R.M. Wentzcovitch, J. Phys.: Condens. Matter. 21 (2009) 395502 (19pp).
[27] J.A. Nelder, R. Mead, Comput. J. 7 (1965) 308. http://dx.doi.org/10.1093/comjnl/7.4.308.
[28] W.H. Press, S.A. Teukolsky, W.T. Vetterling, B.P. Flannery, Numerical Recipes 3rd Edition: The Art of Scientific Computing, third ed., Cambridge University Press, New York, NY, USA, 2007.
[29] See Supplemental material at http://dx.doi.org/10.1016/j.cpc.2015.05.011 for a list of all the calculated lattice constants and bulk moduli. We also list the choice of valence states for the pseudopotentials and provide the input files for the pseudopotential construction.
[30] R.D. Johnson III (Ed.), NIST Computational Chemistry Comparison and Benchmark Database, NIST Standard Reference Database Number 101, Release 16a (August 2013).